doi:10.1017/S1431927622006742
Microsc. Microanal. 28 (Suppl 1), 2022

Detection Limits for Imaging Chiral Magnetic Materials with 4-Dimensional Lorentz Scanning Transmission Electron Microscopy

Xiyue S. Zhang[1], Kayla X. Nguyen[1,2], Emrah Turgut[1,3], Zhen Chen[1], Celesta S. Chang[1], Yu-Tsun Shao[1], Gregory D. Fuchs[1,4], David A. Muller[1,4]*

[1.] School of Applied and Engineering Physics, Cornell University, Ithaca, NY, USA.
[2.] Department of Materials Science and Engineering, University of Illinois Urbana-Champaign, Urbana, IL, USA.
[3.] Taiwan Semiconductor Manufacturing Company, San Jose, CA, USA.
[4.] Kavli Institute at Cornell for Nanoscale Science, Ithaca, NY, USA.
* Corresponding author: David.a.muller@cornell.edu

The Lorentz mode of electron microscopy has been widely used in studying magnetic properties of chiral materials and topological spin textures including helices and magnetic skyrmions [1-3]. However, few investigations on the nanoscale magnetic phenomenon like spin switching in 2D Moiré patterns or chiral magnetic ordering at grain boundaries have been reported with conventional Lorentz methods. The challenge coming from the former is to get a good signal to noise ratio when there are only a few atomic layers of electron spins in the material and the latter is to disentangle the weaker magnetic signal from the strongly-varying grain contrast. We show how to improve the detection limit to address these challenges with 4-dimensional Lorentz scanning transmission electron microscopy (4D-LSTEM) enabled by direct electron detectors such as the electron microscope pixel-array detector (EMPAD) [4]. 4D-LSTEM detects local magnetic field by capturing the beam deflection from Lorentz force in k_x-k_y momentum space at each x-y real space scanning position [5]. The high dynamic range of the EMPAD enables highly sensitive mapping of magnetic fields, simultaneously with the crystalline order without saturating the detector, and thus makes direct imaging of nanoscale chiral magnetic properties in 2D materials and polycrystalline materials possible.

We address the sensitivity challenge by identifying the optimal imaging conditions with quantitative simulations for detecting a single spin with 4D-LSTEM. Fig. 1d shows that the precision is more dependent on the number of electrons than the number of pixels on a detector, stressing the importance of a high-dynamic-range detector. From counting statistics, the minimum required dose is proportional to the square of the ratio between convergence angle and peak deflection angle [6], so we plot center of mass (CoM) line profiles at different convergence angle and beam voltage and determine the trend of the peak deflection. Fig. 1f shows the ratio of peak deflection over convergence angle is proportional to the convergence angle and higher voltage has a higher deflection ratio, suggesting that higher convergence angle and higher voltage are better for optimizing dose (this would not be the case for a uniform field). The minimum required dose for imaging a single spin under 300 kV beam voltage and 35 mrad convergence requires 50 ms/pixel exposure time for a 1 nA current probe, which is close to the detection limit of a field emission scope. This finding enables the possibility of imaging spin textures in materials that are only a few atomic layers thickness at atomic resolution.

We apply our technical approach to disentangle magnetic contrast from grain contrast in a chiral polycrystal FeGe thin film and observe magnetic helicity changes between adjacent grains. We know that the electrostatic potential at the grain boundaries in the sample is a rapid-varying field and results in intensity redistribution in the central disk, and magnetic potential is a slowly varying field and causes a

uniform shift of the central disk [7], and therefore we disentangle contrast from the two effects by performing CoM on only the edge of the central disk. The resulted magnetic field map in Fig. 2b shows the skyrmion vortex has anticlockwise rotation on the top grain and clockwise rotation on the bottom grain, thus showing a helicity inversion across the grain boundary. The crystal chirality also switches in the corresponding grains, as tracked by the tiny rotation of the marked cyan atoms (Ge) relative to the corner yellow atoms (Fe and Ge in projection), where it's clockwise in Fig. 2c and anticlockwise in Fig. 2d. Across another grain boundary where the magnetic induction map shows magnetic helicity is unchanged, HAADF shows the crystal chirality is also preserved. By disentangling magnetic contrast from electrostatic contrast at grain boundaries using 4D-LSTEM, we show magnetic helicity couples to crystal chirality in polycrystal FeGe. [8]

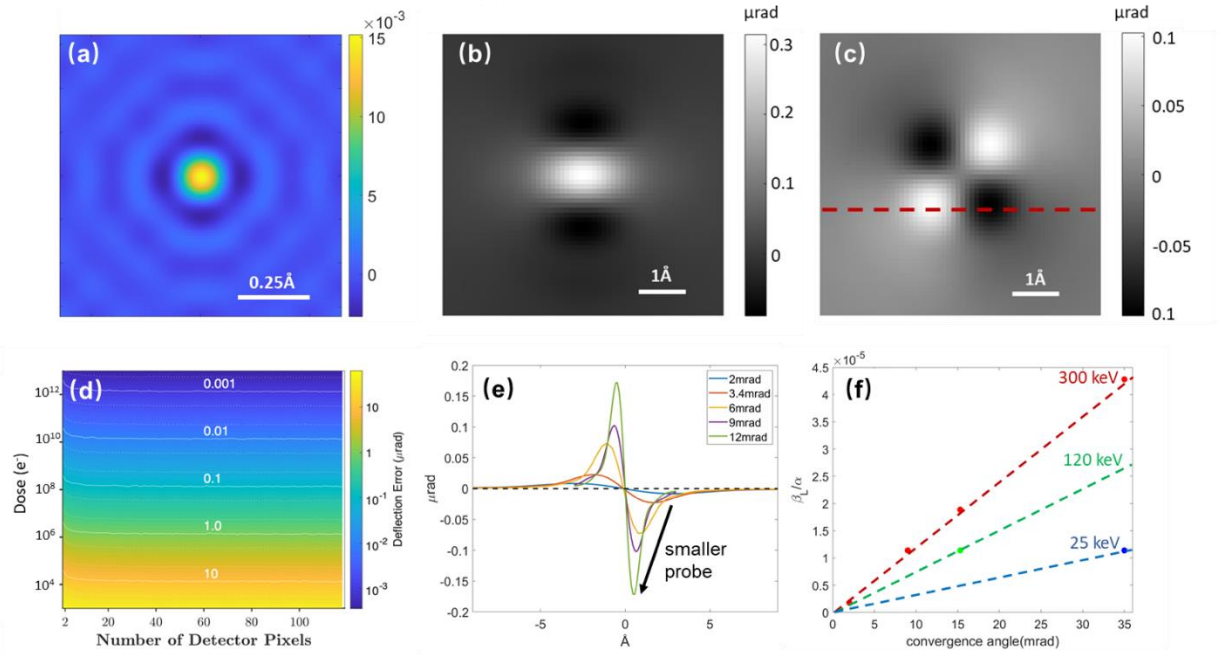

Figure 1. Simulated Center-of-Mass Lorentz 4D-STEM to optimize the sensitivity for detecting a single spin. (a) Simulated initial probe wavefunction at 300 kV, 9 mrad with normalized intensity. (b)&(c) CoM image on simulated 4D-LSTEM datasets on a single spin for the probe in (a) showing contrast from the y-direction disk shift (b) and the x-direction disk shift (c). The signal shape in CoM images matches with deflection angle distribution but broadened after convolution with the probe. (d) Simulations using a 2 mrad semi-convergence angle at a beam energy of 200 keV, and sample thickness of 100 nm showing the minimum measurable deflection angle as a function of electron dose and number of detector pixels. The white lines represent the contours for deflection error as 0.2, 0.5 (dotted lines) and 1 (solid lines) times powers of 10. (e) Line profile of CoMy from the red dashed line in (c) as a function of convergence angles at 300 kV. (f) The ratio of peak deflection over convergence angle is proportional to convergence angle, and increase with increasing voltage, as a consequence of the decreased probe size.

https://doi.org/10.1017/S1431927622006742 Published online by Cambridge University Press

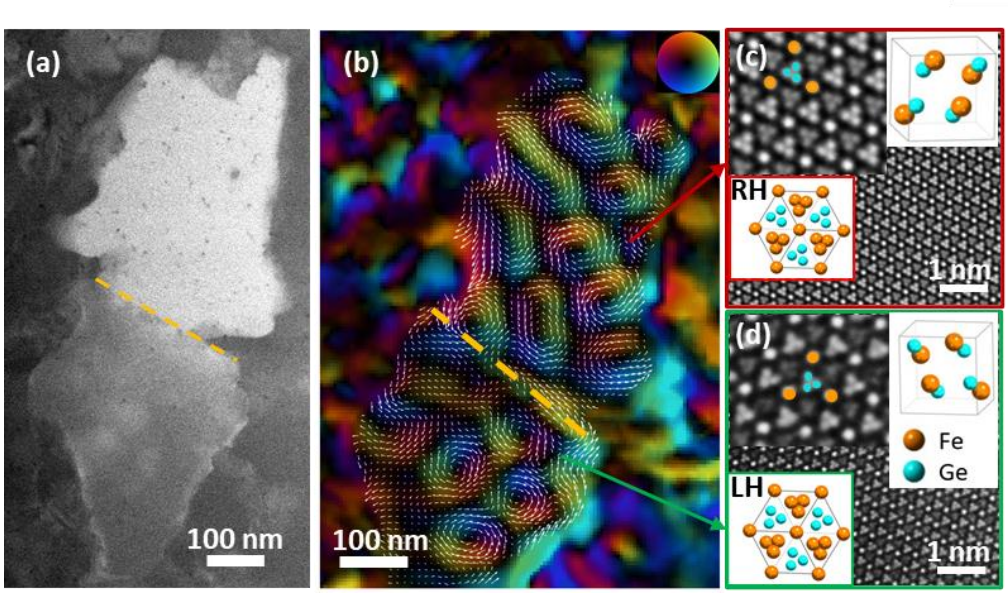

Figure 2. Disentangling magnetic and grain contrast in polycrystal B20-FeGe grains. (a) Annular dark field image shows contrast from two adjacent ~[111]-oriented grains with a grain boundary marked by a yellow dashed line. (b) 4D Lorentz-STEM at 100 K and 130 mT applied field showing skyrmion helicity inverts on the two adjacent grains from right-handed (RH) in the upper grain to left-handed (LH) in the lower. The arrows indicate the direction of the local magnetic field. The continuous color scale in the color wheel refers to different orientation of the magnetic phase and the brightness indicate the amplitude of the field. (c)& (d) are atomic resolution HAADF images with (c) from the top grain and (d) from the bottom grain viewed down the [111] zone axis, showing the reversal of crystal chirality from being RH to LH, as illustrated by the colored atoms and corresponding crystal structure simulation in the insets.

Reference:

[1] K. Shibata *et al.*, Nat Nanotechnol 8, 723 (2013). doi: 10.1038/nnano.2013.174
[2] N. Nagaosa and Y. Tokura, Nat Nanotechnol 8, 899 (2013). doi: 10.1038/nnano.2013.243
[3] X. Z. Yu *et al.*, Nat Mater **10**, 106 (2011). doi: 10.1038/nmat2916
[4] M. W. Tate *et al.*, Microsc Microanal 22, 237 (2016). doi: 10.1017/S1431927615015664
[5] M. Krajnak *et al.*, Ultramicroscopy 165, 42-50 (2016). doi: 10.1016/j.ultramic.2016.03.006
[6] Chapman. J. N., J Phys D Appl Phys [Online]17, 623 (1984), https://iopscience.iop.org/article/10.1088/0022-3727/17/4/003 (Accessed Feb 13, 2022).
[7] M. C. Cao *et al.*, Microscopy (Oxf) 67, i150 (2018). doi: 10.1093/jmicro/dfx123
[8] Funding from the National Science Foundation (DMR-1719875, DMR-2039380), DARPA (D18AC00009) and Department of Energy (DE-SC0012245).